*Human Molecular Genetics*, 2017, Vol. 26, No. 4 729–741

**doi: 10.1093/hmg/ddw413**
Advance Access Publication Date: 23 January 2017
Original Article

ORIGINAL ARTICLE

# The Parkinson's disease-linked protein TMEM230 is required for Rab8a-mediated secretory vesicle trafficking and retromer trafficking

Myung Jong Kim, Han-Xiang Deng, Yvette C. Wong, Teepu Siddique and Dimitri Krainc*

The Ken and Ruth Davee Department of Neurology, Northwestern University Feinberg School of Medicine, Chicago, IL, USA

*To whom correspondence should be addressed at: The Ken and Ruth Davee Department of Neurology, Northwestern University Feinberg School of Medicine, 303 E. Chicago Ave, Ward 12-140, Chicago, IL 60611, USA. Tel: +1-3125033936; Fax: +1-3125033951; Email: suzanne.pressler@northwestern.edu

## Abstract

*TMEM230* is a newly identified Parkinson's disease (PD) gene encoding a transmembrane protein whose cellular and pathogenic roles remain largely unknown. Here, we demonstrate that loss of TMEM230 disrupts retromer cargo CI-M6PR (cation-independent mannose 6-phosphate receptor) trafficking and autophagic cargo degradation rates. TMEM230 depletion further inhibits extracellular secretion of the autophagic cargo p62 and immature lysosomal hydrolases in Golgi-derived vesicles leading to their intracellular accumulation, and is specifically mediated by loss of the small GTPase Rab8a. Importantly, PD-linked TMEM230 variants also induce retromer mislocalization, defective cargo trafficking, and impaired autophagy. Finally, we show that knockdown of another PD gene, LRRK2, which phosphorylates Rab8a, similarly impairs retromer trafficking, secretory autophagy and Golgi-derived vesicle secretion, thus demonstrating converging roles of two PD genes TMEM230 and LRRK2 on Rab8a function, and suggesting that retromer and secretory dysfunction play an important role in PD pathogenesis.

## Introduction

Parkinson's disease (PD) is the second most prevalent neurodegenerative disorder characterized by resting tremors, bradykinesia, rigidity, postural instability as well as additional prodromal non-motor symptoms. PD patients develop early degeneration of substantia nigra pars compacta (SNpc) and Lewy body pathology (1). Previous pedigree studies and large-scale GWAS-study have identified multiple potential susceptibility genes and loci related to PD (2–4). Although the precise pathogenic molecular mechanisms of PD remain under intense investigation, accumulating evidence suggests that oxidative stress and mitochondrial dysfunction, impaired autophagic-lysosomal pathways, and defective vesicle trafficking play important roles in PD pathogenesis (5).

*TMEM230* (Transmembrane Protein 230, also known as C20orf30) was recently identified as a novel PD gene in a large PD family of Northern European ancestry with 81 members (15 affected) and a mean disease onset of 65.5 years (6). Genetic linkage analysis and whole exome sequencing identified R141L as the pathogenic variant in 4 affected individuals which was associated with an autosomal dominant mode of inheritance in this family. Additional PD-linked mutations (Y92C and *184Wext*5) were identified by DNA sequencing of 832 PD samples collected in North America, including 433 familial and 399 sporadic PD cases. Subsequently, an *184PGext*5 mutation in TMEM230 was identified in nine PD patients from seven families with PD in China. Interestingly, the *184PGext*5 mutation was associated with both autosomal dominant and autosomal recessive inheritance in these families (6).

**Received:** July 11, 2016. **Revised:** November 3, 2016. **Accepted:** November 30, 2016

TMEM230 is a putative transmembrane protein with ubiquitous expression and no obvious sequence homology to any other known protein. Ectopically expressed TMEM230 localized with VMAT2-positive vesicles, VPS35-positive endosomes, Rab11-positive recycling endosomes, and Rab5-positive early endosomes, with predominant enrichment in STX-6-positive trans-Golgi network (TGN). Expression of PD-linked TMEM230 mutants led to α-synuclein accumulation and decreased motility of GFP-VAMP2-labelled vesicles. TMEM230 was also found in α-synuclein-positive Lewy bodies and Lewy neurites in the midbrain and neocortex sections from patients with sporadic PD and Dementia with Lewy bodies (DLB) (6).

While the genetic evidence demonstrating TMEM230 as a causative gene for familial PD has been established (6), its normal and pathological cellular functions remain to be elucidated. Here we show that loss of function of TMEM230 impairs secretory autophagy (exophagy), Golgi-derived vesicle secretion and retromer trafficking, which is mediated by loss of Rab8a. Importantly, we also demonstrate retromer and autophagic dysfunction upon expression of PD-linked TMEM230 variants and in PD TMEM230 mutant patient lymphoblastoid cell lines. Finally, we show that knockdown of another PD gene, LRRK2, which has previously been shown to phosphorylate Rab8a (7), similarly impairs secretory autophagy (exophagy) and Golgi-derived vesicle secretion, thus demonstrating converging roles of two PD genes TMEM230 and LRRK2 on Rab8a function. Importantly, these results implicate retromer and secretory dysfunction in TMEM230 and LRRK2-mediated PD pathophysiology.

## Results

### PD-linked R141L TMEM230 variant impairs normal retromer trafficking

Previous immunostaining studies suggested that TMEM230 predominantly localized to the trans-Golgi network and partially co-localized with vacuolar protein sorting-35 (VPS35), a core component of the retromer complex (6). The retromer mediates retrograde vesicular transport of transmembrane proteins from endosomes to the trans-Golgi network (TGN) and the plasma membrane (8–10). To explore the cellular consequences of TMEM230 variants on the intracellular distribution of VPS35, we first expressed wild-type or PD-linked mutants (R141L or *184Wext*5) TMEM230 (Supplementary Material, Fig. S1) together with FLAG-VPS35 in COS-7 cells. Both wildtype TMEM230 and VPS35 showed cytoplasmic distribution with higher immunostaining intensity near the nucleus (Fig. 1A and B). In contrast, the PD-linked R141L-TMEM230 mutant co-localized with VPS35 into a punctate cytoplasmic distribution. In addition, the PD-linked *184Wext*5-TMEM230 mutant also showed robust punctate distribution and co-localized with VPS35 (Fig. 1A and B). These data indicate that PD-linked TMEM230 variants (R141L and *184Wext*5) contribute to altered intracellular distribution of the retromer component VPS35.

The best characterized retromer cargo is the cation-independent mannose 6-phosphate receptor (CI-M6PR) which binds newly synthesized lysosomal hydrolases in the trans-Golgi network (TGN) for delivery to pre-lysosomal compartments (8,11). Defective retromer function is associated with reduced CI-M6PR levels, leading to impaired retrieval of CI-M6PR from endosomes to the TGN and subsequent degradation of CI-M6PR in lysosomes (8,12,13). To examine whether PD-linked TMEM230 variants alter CI-M6PR retromer cargo trafficking, we expressed wildtype or PD-linked R141L-TMEM230 mutant in HEK293-FT cells and examined CI-M6PR protein levels either at steady state or after Baf-A1 treatment to examine lysosomal flux. Baf-A1 acts by inhibiting vacuolar $H^+$ ATPase (V-ATPase) which neutralizes lysosomal pH and therefore inhibits the activity of lysosomal hydrolases (14). At steady state (untreated cells), we observed a significant decrease in CI-M6PR levels in the presence of mutant R141L-TMEM230, as compared to wild-type TMEM230 (Fig. 1C and D). In contrast, R141L-TMEM230 did not disrupt the protein levels of VPS35 either at steady state or upon Baf-A1 treatment (Fig. 1C and E).

To further examine retromer dysfunction in the presence of TMEM230 PD-linked mutants, we tested human lymphoblastoid cell lines derived from PD patients with a heterozygous R141L mutation, as well as two healthy individuals from the same family, and a line derived from an unrelated individual carrying a heterozygous ALS (Amyotrophic Lateral Sclerosis)-linked SPG11 mutation. TMEM230 protein levels were significantly lower in one of the R141L mutant lines compared to healthy controls (Fig. 1F and G). In addition, CI-M6PR protein levels from the two PD TMEM230 mutant patient lines were significantly reduced compared to the lines derived from healthy family members, while the line from the unrelated individual carrying the heterozygous SPG11 mutation did not show a reduction in CI-M6PR (Fig. 1F and H). Taken together, these results suggest that the PD-linked R141L-TMEM230 mutation impairs retromer trafficking.

### TMEM230 regulates autophagy-mediated clearance of p62 and α-synuclein

Increasing evidence suggests that impaired autophagy-lysosomal function plays a key role in the pathogenesis of PD (15). Previously we found increased levels of intracellular α−synuclein upon expression of PD-associated TMEM230 mutants (6). Since α-synuclein is predominantly degraded by the autophagy-lysosomal clearance pathway (16), we next tested whether endogenous TMEM230 regulates the autophagic pathway. For this, we first generated two stable HEK239-FT cell lines that either expressed scrambled-shRNAi or TMEM230-shRNAi (Supplementary Material, Fig. S2). Using carbonyl cyanide *m*-chlorophenylhydrazone (CCCP), a mitochondrial uncoupler known to induce robust autophagic clearance of ubiquitinated substrates (17,18), we monitored CCCP-induced clearance of *SQSTM1*/p62, α-synuclein, and mitofusin 1 (Mfn1). Upon CCCP-treatment, protein levels of p62 and α-synuclein gradually declined in control Scr-RNAi cell line (Fig. 2A–C). However, upon TMEM230 RNAi depletion, the autophagic clearance rates of p62 and α-synuclein were significantly reduced (Fig. 2A–C). Importantly, the CCCP-induced clearance rate of Mfn1, a cargo ubiquitinated by activated Parkin and which undergoes proteasomal rather than autophagic degradation (17), was not altered by TMEM230 depletion (Fig. 2A and D). Interestingly, TMEM230 itself was also reduced upon CCCP treatment in Scr-RNAi cells (Fig. 2A and E). Taken together, these results demonstrate that TMEM230 depletion disrupts efficient CCCP-induced autophagic clearance of both p62 and α-synuclein.

*SQSTM1*/p62 and LC3-II are important for selective targeting of ubiquitinated proteins for lysosomal degradation and accumulate when autophagic flux is impaired (19). To determine how PD-associated TMEM230 variants affect autophagy, we expressed PD-linked TMEM230 mutants (R141L, *184Wext*5 and Y92C) (Fig. 2F and Supplementary Material, Fig. S1) and examined p62 and LC3-II protein levels. In the presence of

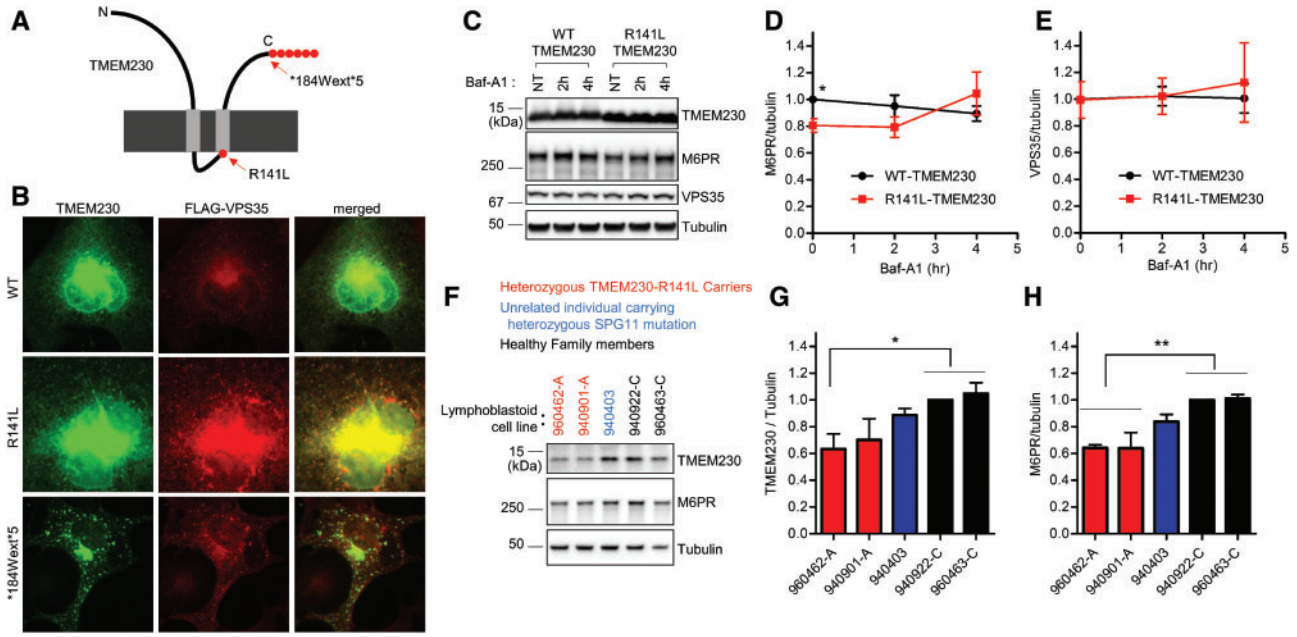


**Figure 1.** PD-linked TMEM230 variants disrupt VPS35 distribution and retromer cargo CI-M6PR trafficking. (**A**) Schematic diagram of TMEM230 mutations from Parkinson's patients. (**B**) Pathogenic PD-linked TMEM230 mutants show more punctate distribution, and alter intracellular distribution of the VPS35 retromer complex. COS-7 cells were transfected with indicated tag-free TMEM230 expression vector together with FLAG-tagged VPS35 expression vector. One day after transfection, COS-7 cells were fixed with 4%formaldehyde in PBS and immunostained with mouse anti-TMEM230 antibody and rabbit anti-FLAG-antibody. Representative images are shown. (**C-E**) PD-linked R141L-TMEM230 mutant reduces steady state levels of CI-M6PR retromer cargo compared to WT-TMEM230. HEK293-FT cells were transfected either with tag-free WT-TMEM230 or R141L-TMEM230. One day after transfection, transfected cells were treated with 300 nM Baf-A1 for indicated times. Cells were then lysed with 2x SDS sample buffer, and analysed with immunoblot analysis using antibodies against TMEM230, CI-M6PR, VPS35, and tubulin. (**C**) Representative immunoblot data from cell lysates. Immunoblot band intensities of CI-M6PR (**D**) and VPS35 (**E**) were normalized to tubulin, and then compared to wild type TMEM230. Data represent mean ± SEM; $N = 3$, two-tailed paired *t*-test, *=$P < 0.05$ compared with WT-TMEM230. (**F–H**) Human lymphoblastoid cell lines harboring the PD-linked R141L TMEM230 mutation have decreased TMEM230 and CI-M6PR levels. Total cell lysate from human lymphoblastoid cell lines derived from two affected PD patients carrying heterozygous R141L mutations, one unrelated individual carrying an ALS-linked heterozygous SPG11 mutation, and two healthy family members were analysed with immunoblotting using indicated antibodies. Band intensities of TMEM230 (**G**) and CI-M6PR (**H**) were normalized to tubulin, and then compared to a lymphoblastoid cell line from healthy family member (lymphoblastoid cell line-940922-C). Data represent mean ± SEM; $N = 4$, one-way ANOVA with Tukey's multiple comparison test, *=$P < 0.05$; **=$P < 0.01$.

PD-associated TMEM230 mutants, intracellular levels of both p62 and LC3-II levels were increased, as compared with wild-type TMEM230 (Fig. 2G–I), further suggesting that PD-associated TMEM230 mutants disrupt autophagy.

## TMEM230 regulates retromer trafficking and secretory autophagy

Thus far, we have demonstrated that PD-associated TMEM230 variants disrupt both retromer trafficking and autophagy. These findings raise the question as to whether endogenous TMEM230 normally regulates these pathways. First, to examine endogenous TMEM230's role in retromer trafficking, we expressed either Scr-RNAi or TMEM230-RNAi in HEK293-FT cells for two days to knockdown TMEM230 levels (Fig. 3A), and examined the levels of the retromer cargo CI-M6PR. Similar to what was observed upon expression of TMEM230 PD-linked R141L mutant (Fig. 1D), RNAi knockdown of TMEM230 reduced steady state levels of CI-M6PR (Fig. 3A and B), suggesting that TMEM230 normally regulates the retromer trafficking of CI-M6PR, and that the R141L mutation leads to partial TMEM230 loss of function.

Next, we examined endogenous TMEM230's role in autophagy by examining autophagic flux using Baf-A1 to inhibit lysosomal hydrolases. Importantly, TMEM230 knockdown by RNAi led to a significant accumulation of p62 and LC3-II upon Baf-A1 treatment (Fig. 3A,C and D). Baf-A1 acts by inhibiting vacuolar H+ ATPase (V-ATPase) in lysosomes and neutralizing lysosomal pH (14), which induces lysosomal calcium release and the induction of various secretory trafficking events, including lysosomal exocytosis (20), Golgi-derived vesicle secretion (21,22), and secretory autophagy (also known as exophagy) (23–28). To investigate whether TMEM230 depletion misregulates extracellular secretion of p62, we analysed p62 protein levels in the extracellular media fractions after Baf-A1 treatment. Interestingly, we found that Baf-A1 treatment in cells caused robust p62 secretion into extracellular media, but was dramatically impaired by TMEM230 depletion (Fig. 3I and J), suggesting that TMEM230 dysfunction results in p62 accumulation due to defective secretory autophagy.

As our previous study showed predominant TMEM230-eGFP enrichment in the STX-6 positive TGN, we also investigated whether TMEM230 might regulate the secretion of Golgi-derived vesicles. To test this, we examined the intracellular and secreted levels of immature lysosomal hydrolases which are cargo of Golgi-derived vesicles, and compared them to levels of mature lysosomal hydrolases which localize to lysosomes. In control cells, Baf-A1 led to the gradual extracellular secretion of both immature (i-Cat-D and i-HEX-B) and mature (m-Cat-D and m-HEX-B) forms of the lysosomal hydrolases

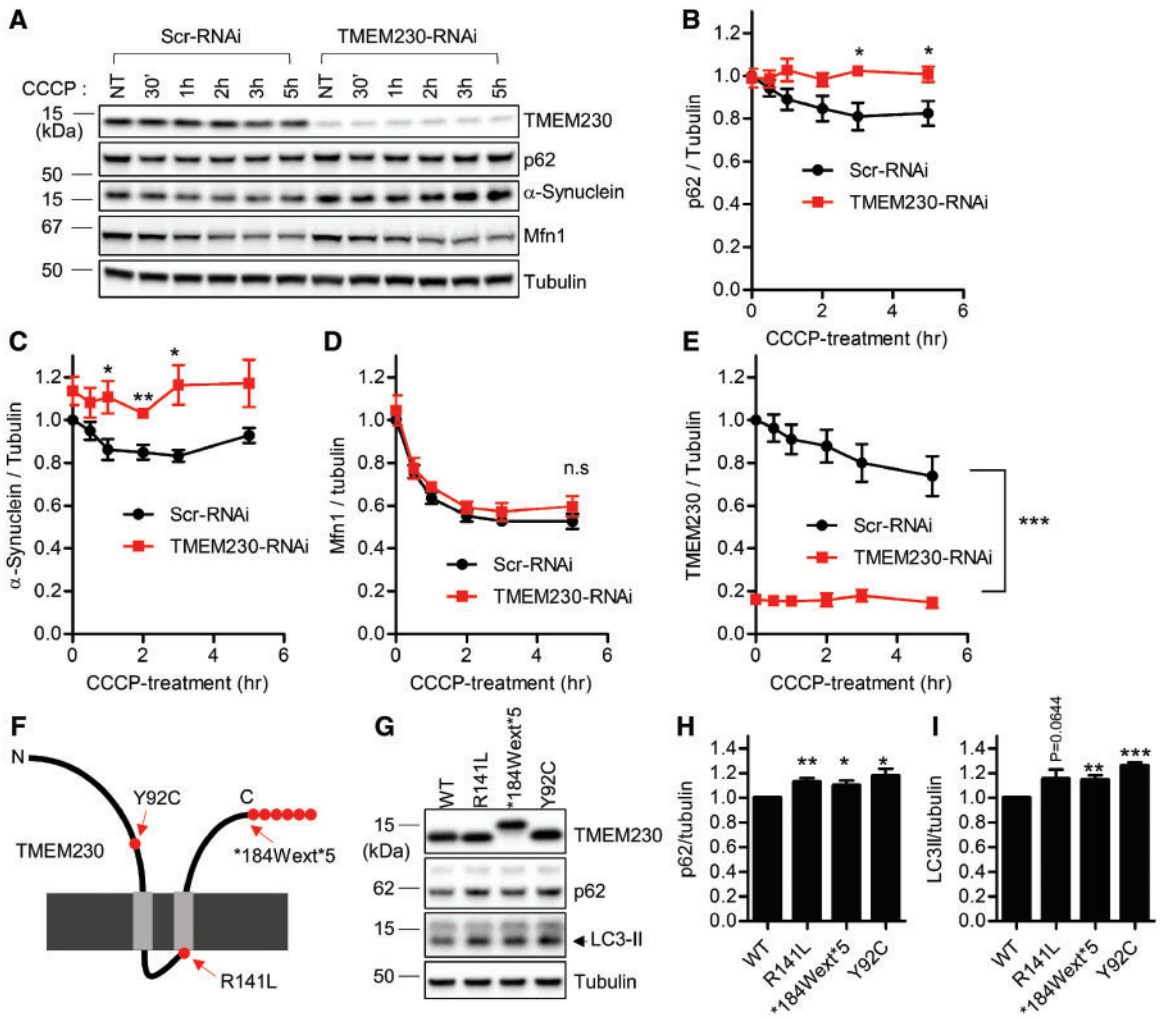


**Figure 2.** PD-linked TMEM230 variants and TMEM230 knockdown disrupt autophagic clearance of p62 and α-synuclein. (**A–E**) Knockdown of endogenous TMEM230 impairs CCCP-induced autophagic clearance of p62 and α-synuclein. (**A**) Stable HEK293-FT cell lines expressing either control Scr-RNAi or TMEM230-RNAi were treated with 5 μM CCCP for the indicated time. Cells were then lysed with 2X SDS sample buffer, and analysed with immunoblotting using indicated antibodies. Immunoblot band intensities were normalized to tubulin, and compared to control Scr-RNAi cells. Graphs show normalized immunoblot band intensities of p62 (**B**), α-synuclein(**C**), Mfn1 (**D**) and TMEM230 (**E**). Data represent mean ± SEM; $N = 5$, two-tailed paired *t*-test; *=$P < 0.05$; **=$P < 0.01$; ***=$P < 0.001$. (**F-H**) PD-linked TMEM230 mutants induce increased intracellular p62 and LC3-II levels, compared to wild type TMEM230. HEK293-FT cells were transfected with indicated tag-free TMEM230 expression vectors. Two days after transfection, cells were lysed with 2X SDS sample. Cell lysates were analysed with immunoblot analysis using indicated antibodies. Immunoblotting band intensities were normalized with tubulin band intensity, and compared to wild type TMEM230. Graphs show normalized band intensities of p62 (**H**) and LC3-II (**I**). Data represent mean ± SEM, $N > 5$, two-tailed paired *t*-test, *=$P < 0.05$; **=$P < 0.01$; ***=$P < 0.001$ compared with WT-TMEM230.

cathepsin-D and hexosaminidase B (Fig. 3I and K–N). However, TMEM230 depletion only delayed the secretion rate of immature forms of lysosomal hydrolases (i-HEX-B and i-Cat-D) (Fig. 3I, K and M), concomitant with an increase in their intracellular accumulation in corresponding cell lysates (Fig. 3A, E and G). In contrast, TMEM230 depletion did not disrupt the secretion rate of mature forms of lysosomal hydrolases (m-Cat-D and m-HEX-B) (Fig. 3I, L and N) or the rate of change in their intracellular levels upon Baf-A1 treatment (Fig. 3A, F and H). As immature forms of lysosomal hydrolases preferentially localize to Golgi-derived vesicles, these results indicate that in addition to regulating retromer trafficking and secretory autophagy, TMEM230 regulates the extracellular secretion of Golgi-derived vesicles.

## Rab8a mediates TMEM230 regulation of retromer trafficking and the secretory pathway

Next, we asked how TMEM230 depletion might impair secretory autophagy and the secretion of Golgi-derived vesicles. The Rab family of small GTPases plays pivotal roles in various steps of vesicular trafficking in cells (29,30). Among these, Rab8a GTPase has been previously implicated in both secretory autophagy (exophagy) (23,28) and *trans*-Golgi network to plasma membrane trafficking (31). Given these previously studied cellular roles of Rab8a, we tested whether Rab8a might mediate the cellular defects we observed upon TMEM230 loss of function. Interestingly, TMEM230 depletion led to a significant reduction in Rab8a protein levels in cells (Fig. 4A). In contrast, protein levels of Rab7a, a small GTPase implicated in endo-lysosomal trafficking, early-to-late

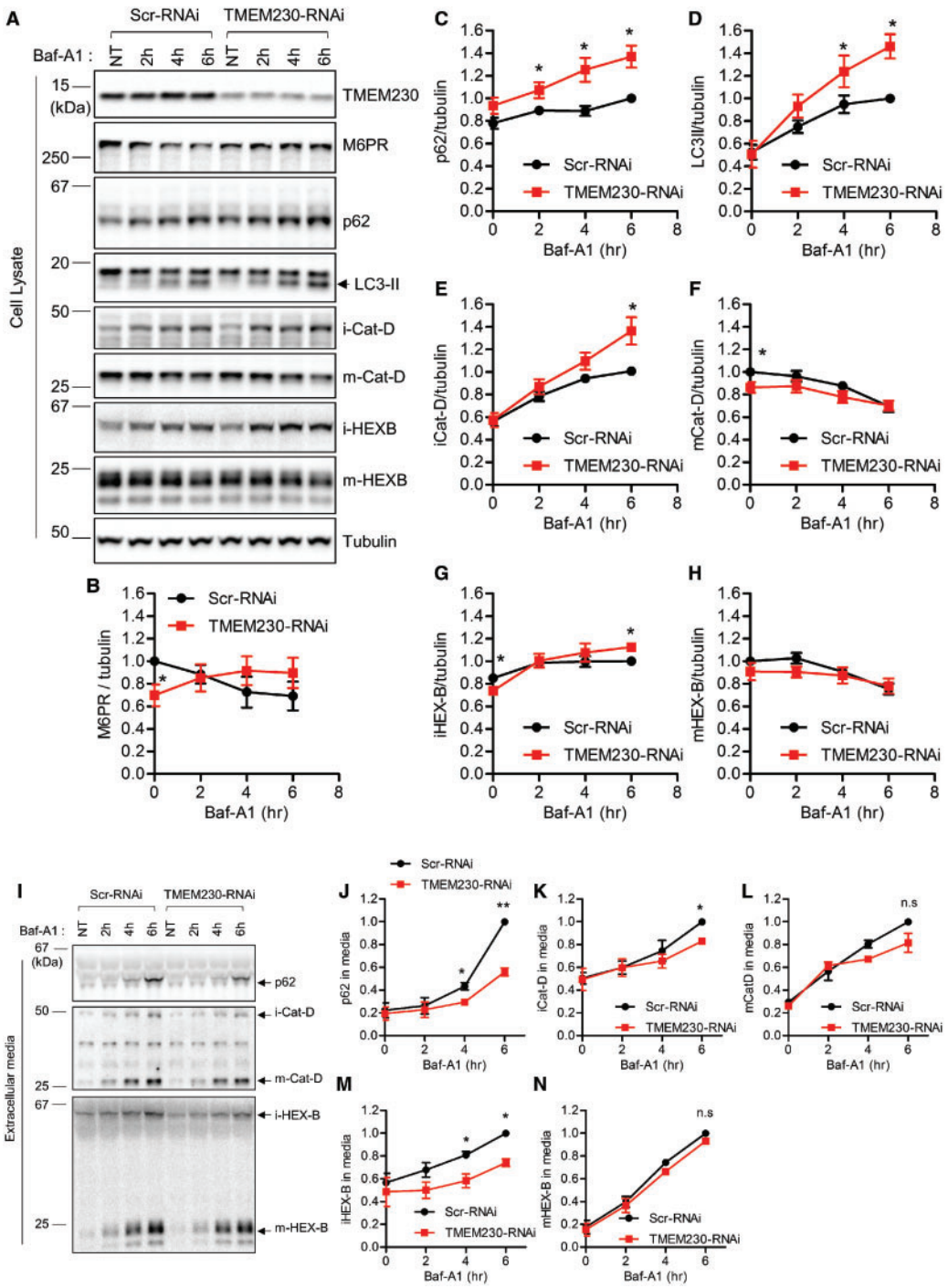


**Figure 3.** TMEM230 knockdown disrupts retromer cargo CI-M6PR trafficking and impairs secretory autophagy and Golgi-derived vesicle secretion. (**A–H**) TMEM230 depletion reduces steady state levels of CI-M6PR retromer cargo levels and increases BafA1-induced intracellular accumulation of autophagic cargo (p62 and LC3-II) and Golgi-derived vesicle cargo (immature lysosomal hydrolases iCat-D and iHEX-B) but not lysosomal cargo (mature lysosomal hydrolases mCat-D and mHEX-B). HEK293-FT cells were transfected with either control Scr-RNAi or TMEM230-RNAi. Two days later, cells were treated with 300 nM Baf-A1 for the indicated time. Cell lysates fractions and extracellular media fraction were prepared as described in Experimental Procedures. Protein samples from cell lysate were analysed with immunoblotting with indicated antibodies. (**A**) Representative immunoblot data from cell lysates. Band intensities were normalized to tubulin, and compared to control Scr-RNAi. Graphs show normalized band intensities of intracellular CI-M6PR ($N = 4$) (**B**), intracellular p62 ($N = 5$) (**C**), intracellular LC3-II ($N = 5$) (**D**), intracellular immature cathepsin-D ($N = 5$) (**E**), intracellular mature cathepsin-D ($N = 5$) (**F**), intracellular immature HEX-B ($N = 5$) (**G**) and intracellular mature HEX-B ($N = 5$) (**H**). Data represent mean ± SEM; two tailed paired *t*-test, *=$P < 0.05$ compared with Scr-RNAi. (**I-N**) TMEM230 depletion inhibits BafA1-induced extracellular secretion of autophagic cargo (p62) and Golgi-derived vesicle cargo (immature lysosomal hydrolases iCat-D and iHEX-B) but not lysosomal cargo (mature lysosomal hydrolases mCat-D and mHEX-B). After Baf-A1 treatment for indicated times, harvested extracellular media fractions were analysed with immunoblotting using indicated antibodies. Band intensities from immunoblotting using conditioned media were normalized to total tubulin in cell lysate fractions, and compared to Scr-RNAi. (**I**) Representative immunoblot data from extracellular media fractions. Graphs show normalized immunoblot band intensities of p62 from extracellular media (**J**), immature cathepsin-D from extracellular media (**K**), mature cathepsin-D from extracellular media (**L**), immature HEX-B from extracellular media (**M**) and mature HEX-B from extracellular media (**N**). Data represent mean ± SEM; $N = 3$, two-tailed paired *t*-test, *=$P < 0.05$; **=$P < 0.01$, compared with Scr-RNAi.

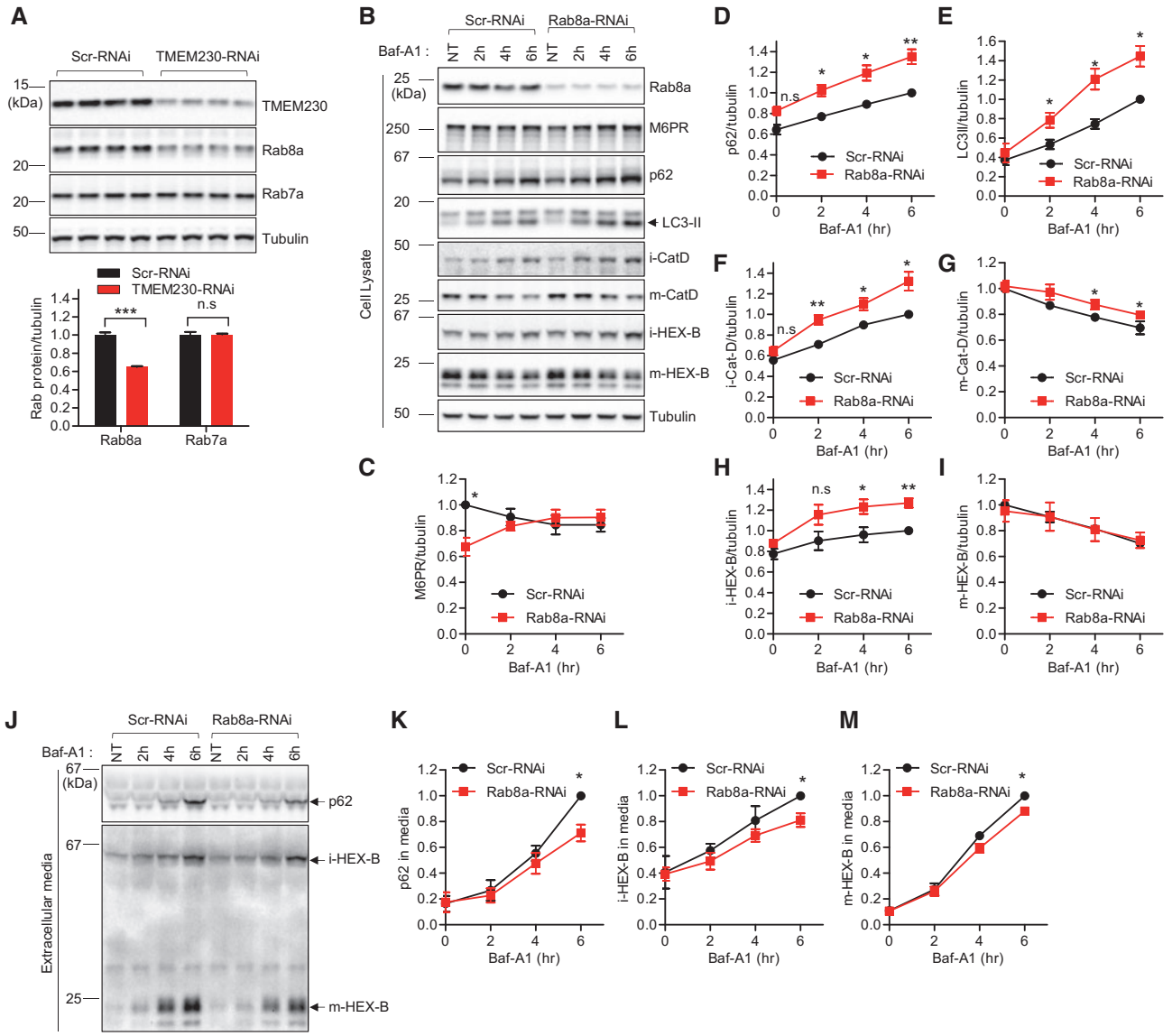


**Figure 4.** Rab8a mediates retromer cargo CI-M6PR trafficking, secretory autophagy and Golgi-derived vesicle secretion defects upon TMEM230 knockdown. (**A**) TMEM230 depletion reduces Rab8a but not Rab7a protein levels. HEK293-FT cells were transfected either with control Scr-RNAi or TMEM230-RNAi. Two days later, transfected cells were analysed with immunoblotting using TMEM230, Rab8a, Rab7a and tubulin antibodies. Immunoblot band intensities were normalized to tubulin, and compared to Scr-RNAi. Graphs show normalized Rab8a immunoblot intensity in cell lysates. Data represent mean ± SEM; $N = 4$, two-tailed *t*-test, ***$=P < 0.001$ compared to Scr-RNAi. (**B-I**) Rab8a depletion reduces steady state levels of CI-M6PR retromer cargo levels and increases BafA1-induced intracellular accumulation of autophagic cargo (p62 and LC3-II) and Golgi-derived vesicle cargo (immature lysosomal hydrolases iCat-D and iHEX-B), and partially affects lysosomal cargo levels (mature lysosomal hydrolases mCat-D and mHEX-B). HEK293-FT cells were transfected with either Scr-RNAi or Rab8a-RNAi. Two days later, cells were treated with 300 nM Baf-A1 for the indicated time. Extracellular media fractions were prepared as described in Experimental Procedures. Cells were lysed with 2X SDS-sample buffer and cell lysates were analysed by immunoblotting with indicated antibodies. (**B**) Representative immunoblot data from cell lysates. Band intensities were normalized to total tubulin, and compared to Scr-RNAi. Graphs show normalized band intensities of intracellular CI-M6PR ($N = 5$) (**C**), intracellular p62 ($N = 5$) (**D**), intracellular LC3-II ($N = 5$) (**E**), intracellular immature cathepsin-D ($N = 5$) (**F**), intracellular mature cathepsin-D ($N = 5$) (**G**), intracellular immature HEX-B ($N = 5$) (**H**) and intracellular mature HEX-B ($N = 5$) (**I**). Data represent mean ± SEM; two-tailed paired *t*-test, *$=P < 0.05$; **$=P < 0.01$ compared with Scr-RNAi. (**J-M**) Rab8a depletion inhibits Baf-A1-induced extracellular secretion of autophagic cargo (p62), Golgi-derived vesicle cargo (immature lysosomal hydrolase iHEX-B) and lysosomal cargo (mature lysosomal hydrolase mHEX-B). After Baf-A1 treatment for indicated times, harvested extracellular media fractions were analysed with immunoblotting using indicated antibodies. (**J**) Representative immunoblot data from extracellular media fractions. Blot band intensities were normalized to total tubulin, and compared to Scr-RNAi. Graphs show normalized immunoblot band intensities of p62 from extracellular media ($N = 3$) (**K**), immature HEX-B from extracellular media ($N = 4$) (**L**), and mature HEX-B from extracellular media ($N = 4$) (**M**). Data represent mean ± SEM; two-tailed paired *t*-test, *$=P < 0.05$, compared with control Scr-RNAi.

endosomal maturation, endosomal positioning, and retromer trafficking, were not changed in TMEM230 depleted cells (Fig. 4A).This finding raised the question of whether the secretory dysfunctions observed in TMEM230 knockdown cells might be due to functional loss of Rab8a.

To test this, we depleted endogenous Rab8a in HEK293-FT cells using RNAi. We found that Rab8a depletion accelerated Baf-A1 induced intracellular accumulation of p62 and LC3-II (Fig. 4B, D and E), concomitant with impaired extracellular secretion of the autophagic cargo p62 (Fig. 4J and K). In addition,

Rab8a depletion accelerated the intracellular accumulation of immature forms of lysosomal hydrolases (i-Cat-D and i-HEX-B) upon Baf-A1 treatment (Fig. 4B, F and H), and inhibited their secretion into extracellular media (Fig. 4J and L). Thus, these results further corroborate the critical involvement of Rab8a in secretory autophagy and support an additional role for Rab8a in regulating the extracellular secretion of Golgi-derived vesicles, similar to what was observed upon TMEM230 loss of function.

To further confirm a role for Rab8a in secretory vesicle trafficking, we examined whether dominant negative Rab8a (T22N) expression had similar effects on the secretion of p62 and lysosomal hydrolases by expressing either GFP-tagged wild type Rab8a (WT-GFP-Rab8a) or GFP-tagged dominant negative T22N Rab8a (T22N-GFP-Rab8a) in HEK283-FT cells treated with or without Baf-A1. We found that consistent with the results from Rab8a depletion, dominant negative Rab8a T22N expression accelerated intracellular accumulation of both p62 and LC3-II upon Baf-A1 treatment (Supplementary Material, Fig. S3A–C) while inhibiting extracellular secretion of p62 (Supplementary Material, Fig. S3H and I). In addition, Rab8a T22N also accelerated the intracellular accumulation of immature forms of lysosomal hydrolases (i-Cat-D and i-HEX-B) upon Baf-A1 treatment (Supplementary Material, Fig. S3A, D and F), and inhibited their secretion into extracellular media (Supplementary Material, Fig. S3H, J and L). Thus, consistent with Rab8a depletion, dominant negative Rab8a had similar effects on both secretory autophagy and Golgi-derived vesicle secretion as TMEM230 loss of function.

Interestingly, we found that Rab8a depletion also had a small but significant effect on inhibiting the secretion of mature lysosomal hydrolases (Fig. 4J and M), with little or no effect on their intracellular accumulation (Fig. 4B, G and I), suggesting that Rab8a may additionally indirectly regulate lysosomal secretion. These results were also observed upon expression of dominant negative T22N-GFP-Rab8a (Supplementary Material, Fig. S3A, E, G, H, K and M).

Finally, as TMEM230 depletion and PD-linked mutants both disrupted steady-state levels of the retromer cargo CI-M6PR (Figs 1D and 3B), we wondered if Rab8a depletion might also mediate TMEM230-induced retromer dysfunction. Consistent with TMEM230 loss of function, we found that Rab8a depletion similarly reduced CI-M6PR protein levels at steady state and causes a trend towards increased accumulation of CI-M6PR upon treatment with Baf-A1 (Fig. 4B and C), indicative of abnormal trafficking of CI-M6PR retromer cargo into lysosomes. These results uncover a novel role for Rab8a in CI-M6PR retromer cargo trafficking, and further suggest that Rab8a mediates both retromer trafficking and secretory dysfunction upon TMEM230 loss of function.

## Loss of PD-linked LRRK2 also disrupts retromer trafficking and the secretory pathway

Autosomal dominant mutations in leucine-rich repeat kinase (LRRK2) are one of the most common genetic causes of late-onset PD (32,33). However, the LRRK2 disease-initiating mechanism is still unclear due to the lack of understanding of bona fide LRRK2 kinase substrates. Recently, an unbiased phosphoproteomic study revealed that LRRK2 phosphorylates a subset of Rab GTPases (Rab3, Rab8a, Rab10 and Rab12), suggesting that LRRK2 might regulate Rab-mediated vesicle trafficking (7). In particular, LRRK2 was shown to interact with Rab8a, while the PD-associated LRRK2 variant (G2019S-LRRK2) increased Rab8a Thr-72 phosphorylation which inhibited Rab8a's interaction with the Rab-GDI complex, resulting in an altered membrane-cytosol distribution of Rab8a (7). Based on this recent study, we hypothesized that properly regulated kinase activation of LRRK2 might be critical for the proper activation cycle of Rab8a in cells, and that G2019S-LRRK2 might slow down the activation cycle of Rab8a by shifting the balance towards phosphorylated Rab8a accumulation in membrane compartments, leading to net inhibition of Rab8a-promoted vesicle trafficking. Supporting this idea, G2019S-LRRK2 has been reported to impair retromer trafficking (34), resulting in reduced CI-M6PR protein levels, although the underlying mechanism remains elusive.

To further examine a role for endogenous LRRK2 in regulating retromer trafficking, we depleted endogenous LRRK2 with RNAi and examined CI-M6PR retromer cargo levels. Consistent with our observations with TMEM230 and Rab8a depletion (Figs 3B and 4C), knockdown of endogenous LRRK2 also reduced basal CI-M6PR levels, and induced progressive accumulation of the CI-M6PR protein upon Baf-A1 treatment (Fig. 5A and B). We also confirmed that G2019S-LRRK2 expression reduced basal CI-M6PR protein levels, compared to wildtype LRRK2 (data not shown). Since both G2019S-LRRK2 expression and LRRK2-knockdown lead to reduced CI-M6PR protein levels in cells, these results suggest that the G2019S-LRRK2 variant may lead to loss of endogenous LRRK2 function resulting in defective retromer trafficking.

As depletion of endogenous TMEM230 disrupted both retromer trafficking as well as the secretion of autophagic cargo (p62) and Golgi-derived vesicle cargo (immature lysosomal hydrolases), we wondered if LRRK2 might also misregulate the secretory pathway. Although LRRK2 depletion did not disrupt Baf-A1 induced LC3-II accumulation (Fig. 5A and D), we found that consistent with TMEM230 depletion, LRRK2 depletion induced a significant increase in Baf-A1 induced intracellular p62 accumulation (Fig. 5A and C), corresponding to a drastic inhibition of p62 secretion into extracellular media (Fig. 5J and K). Thus, endogenous LRRK2 may also regulate the efficient processing of secretory autophagy.

Consistent with TMEM230 depletion, LRRK2 knockdown also led to the accelerated intracellular accumulation of immature lysosomal hydrolases upon Baf-A1 treatment (Fig. 5A, E and G), corresponding to a decreased rate of extracellular secretion (Fig. 5J and L). Furthermore, consistent with TMEM230 depletion, LRRK2 depletion did not alter intracellular levels of Baf-A1 treated mature forms of lysosomal hydrolases (Fig. 5A, F and H) or their secretion into extracellular media (Fig. 5J and M). Thus, endogenous LRRK2 also regulates the extracellular secretion of Golgi-derived vesicles consistent with TMEM230 function. Taken together, these results demonstrate that both PD-associated genes TMEM230 and LRRK2 regulate efficient retromer trafficking, secretory autophagy, and Golgi-derived vesicle secretion.

Finally, we examined the interactions between TMEM230, LRRK2 and Rab8a levels. As TMEM230 depletion decreased Rab8a levels (Fig. 4A), we examined if LRRK2 might similarly affect Rab8a levels. We found that while LRRK2 did not disrupt Rab8a levels at steady state, LRRK2 depletion led to the accelerated Baf-A1 accumulation of Rab8a in cells (Fig. 5A and I), suggesting that both TMEM230 and LRRK2 may disrupt Rab8a homeostasis. We also examined whether TMEM230 levels are altered by either Rab8a or LRRK2. Interestingly, we found that while LRRK2 depletion had no effect on TMEM230 levels (Supplementary Material, Fig. S4A), Rab8a depletion led to a slight increase in TMEM230 levels (Supplementary

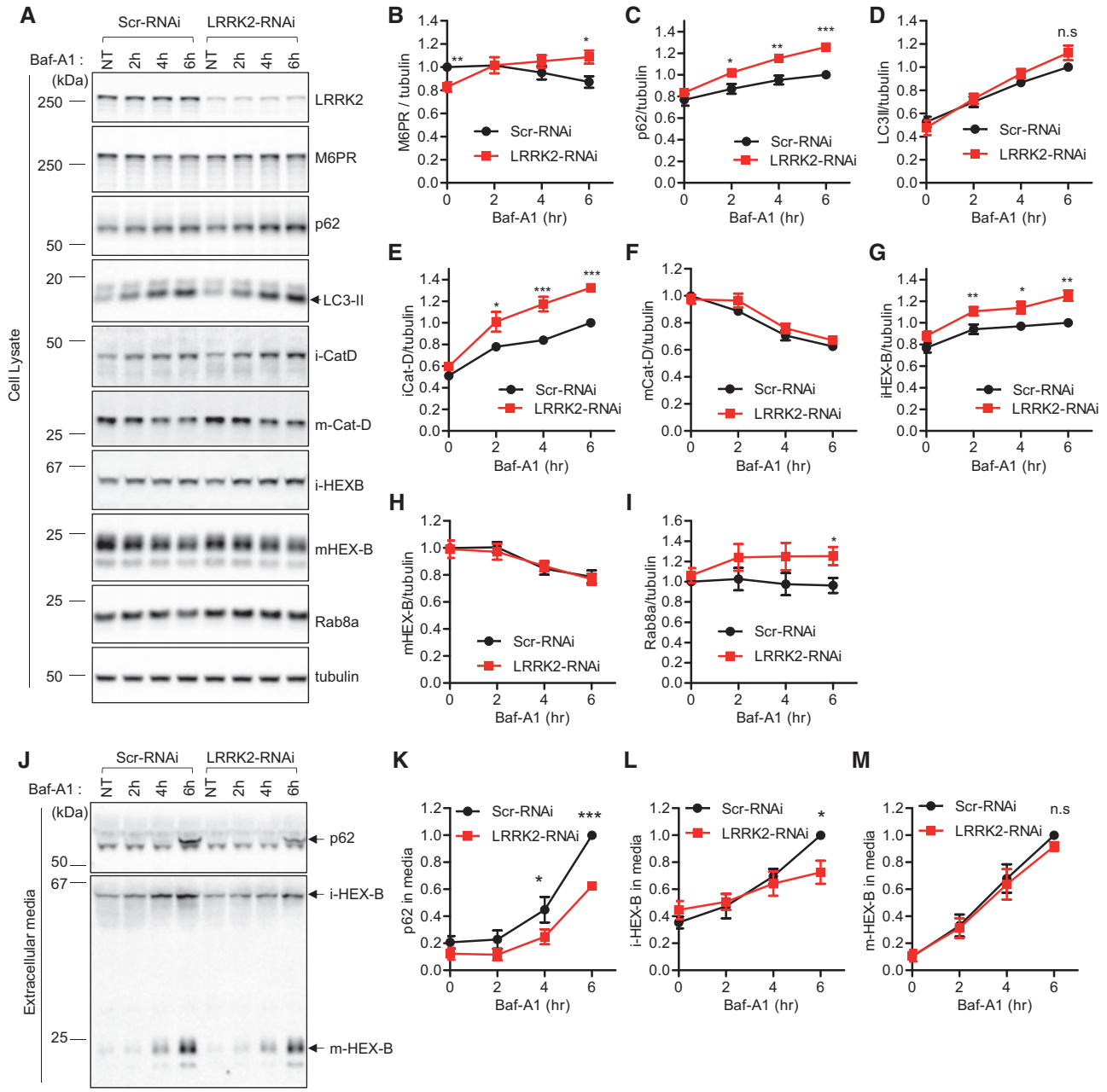


**Figure 5.** Knockdown of LRRK2 disrupts retromer cargo CI-M6PR trafficking and impairs secretory autophagy and Golgi-derived vesicle secretion. (**A–I**) LRRK2 depletion reduces steady state levels of CI-M6PR retromer cargo levels and increases Baf-A1-induced intracellular accumulation of autophagic cargo (p62) and Golgi-derived vesicle cargo (immature lysosomal hydrolases iCat-D and iHEX-B) but not lysosomal cargo (mature lysosomal hydrolases mCat-D and mHEX-B). LRRK2 depletion also increases Baf-A1 induced Rab8a intracellular accumulation. HEK293-FT cells were transfected with either Scr-RNAi or LRRK2-RNAi. Two days after transfection, cells were untreated or treated with Baf-A1 for the indicated times. Extracellular media fractions from each time point were collected, and cells were lysed with 2X SDS sample buffer. Cell lysate samples were analysed with immunoblot analysis using indicated antibodies. Blot band intensities were normalized to tubulin, and compared to control Scr-RNAi. (**A**) Representative immunoblot data from cell lysates. Graphs show normalized band intensities of intracellular CI-M6PR ($N = 7$) (**B**), p62 ($N = 7$) (**C**), LC3-II ($N = 8$) (**D**), immature cathepsin-D ($N = 8$) (**E**), mature cathepsin-D ($N = 8$) (**F**), immature HEX-B ($N = 6$) (**G**), mature HEX-B ($N = 6$) (**H**) or Rab8a ($N = 3$) (**I**). Data represent mean ± SEM; two-tailed paired *t*-test, *=$P < 0.05$; **=$P < 0.01$; ***=$P < 0.001$ compared with control Scr-RNAi. (**J-M**) LRRK2 depletion inhibits Baf-A1-induced extracellular secretion of autophagic cargo (p62) and Golgi-derived vesicle cargo (immature lysosomal hydrolase iHEX-B) but not lysosomal cargo (mature lysosomal hydrolase mHEX-B). After Baf-A1 treatment for indicated times, harvested extracellular media fractions were analysed with immunoblotting using indicated antibodies. (**J**) Representative immunoblot data from extracellular media fractions. Blot band intensities were normalized to total tubulin, and compared to control Scr-RNAi. Graphs show normalized immunoblot band intensities of p62 from extracellular media ($N = 3$) (**K**), immature HEX-B from extracellular media ($N = 4$) (**L**), and mature HEX-B from extracellular media ($N = 4$) (**M**). Data represent mean ± SEM; two-tailed paired *t*-test, *=$P < 0.05$; ***=$P < 0.001$ compared with control Scr-RNAi.

Material, Fig. S4B). Collectively, our results demonstrate a novel pathway for regulating cellular homeostasis in which LRRK2 and TMEM230 both regulate retromer trafficking and Rab8a-mediated secretory autophagy and extracellular secretion of Golgi-derived vesicles, and support a model in which PD-associated mutations in either protein lead to cellular dysfunction via retromer and secretory pathway dysfunction.

## Discussion

Mutations in TMEM230 were recently identified as a novel cause for familial PD (6), but TMEM230's normal cellular functions and the role of pathological PD-linked TMEM230 variants in PD pathogenesis have not been previously defined. In this study, we demonstrate novel roles for TMEM230 in retromer trafficking, secretory autophagy and Golgi-derived vesicle secretion, and show that PD-linked variants may contribute to retromer and autophagic pathway dysfunction.

Endolysosomal dysfunction has previously been implicated in PD pathogenesis, and mutations in multiple PD genes including *LRRK2*, *Parkin*, *ATP13A2* and *VPS35* have been associated with defects in the endolysosomal pathway (15,35). In addition, defective autophagy has been linked to multiple PD genes (36–38) supported by mounting evidence demonstrating the importance of autophagy in PD (37,39–44). However, the molecular details of endolysosomal and autophagic pathway dysfunction in PD pathogenesis have still not been fully elucidated.

Here, we report that the novel PD gene TMEM230 is critical for Rab8a-mediated secretory autophagy and Golgi-derived vesicle secretion. This novel functional connection between TMEM230 and Rab8a, a small GTPase implicated in secretory autophagy and TGN to plasma membrane trafficking, may thus be critical for further understanding the pathophysiological mechanisms in PD as previous studies have mainly focused on degradative autophagy, rather than on secretory autophagy.

Previous biochemical evidence implicate the involvement of Rab8a in the pathogenesis of PD. Rab8a is known to interact with the C-terminal region of α-synuclein (45). LRRK2, the most common late onset familial PD gene, interacts with and phosphorylates Rab8a (7). Furthermore, another recent phosphoproteomic study also revealed possible interactions between Rab8a and the PD-gene PINK1, as the most PINK1-responsive phospho-peptides included equivalent pSer111 phosphopeptides from Rab8A, Rab8B and Rab13, although these Rab proteins were not directly phosphorylated by PINK1 (46). In rat primary neurons overexpressing α-synuclein, over-expression of Rab8a has also been reported to rescue cell death (47). Moreover, overexpression of Rab8a, along with other Rab GTPases promotes the secretion of α-synuclein through secretory autophagy (25), which may contribute to its cell-to-cell propagation in addition to other secretory pathways including exosome secretion (48–50), conventional secretion from the Golgi (51), and brefeldin-A-insensitive non-conventional secretion (52). Interestingly, mutations in α-synuclein, LRRK2, and TMEM230, which are all functionally linked to Rab8a, cause α-synuclein-positive Lewy-body formation (6,53–55). Although secretory autophagy is largely unexplored in the PD-field, our work suggests that it may be a new area to investigate further for its relevance to PD pathogenesis.

TMEM230 predominantly localizes to the trans-Golgi network, endosome structures and synaptic vesicles (6), suggesting a possible role in the trafficking of these organelles. Indeed, Rab8a also promotes membrane traffic from the TGN to the plasma membrane, without affecting ER to Golgi transport (31). Here we demonstrate that in addition to regulating secretory autophagy, TMEM230 also regulates Golgi-derived vesicle secretion of immature lysosomal hydrolases. Thus, we propose that TMEM230 depletion leads to Rab8a loss of function, resulting in defects in both secretory autophagy and Golgi-derived vesicle secretion.

LRRK2 has also previously been implicated in the regulation of the autophagy–lysosomal pathway, as LRRK2 knockout mice display striking accumulation and aggregation of the autophagic cargo p62, α-synuclein and ubiquitinated proteins at 20 months of age (42,56). Although disruption of protein degradation contributes to these defects, impaired secretory autophagy may further exacerbate the accumulation of these proteins. Here, we demonstrate that knockdown of endogenous LRRK2 impairs secretory autophagy, evidenced by hampered p62 secretion into extracellular media, suggesting that dysfunctional secretory autophagy may further contribute to protein accumulation in LRRK2 knockout mice. Previously, Beilina et al. reported that LRRK2 promotes Golgi-derived vesicle clearance through the degradative autophagy-lysosomal pathway (57). Here we show that LRRK2 knockdown also inhibits Golgi-derived vesicle secretion into extracellular media, providing another mechanism for how LRRK2 may promote Golgi-derived vesicle turnover.

Another key finding from this study is that TMEM230 contributes to the regulation of retromer trafficking. The retromer complex mediates endosome to trans-Golgi retrieval of CI-M6PR and other retromer cargo receptors (8,12,13,58). Dysfunctional retromer trafficking is known to cause abnormal flow of retromer cargo to the lysosome and abnormal lysosomal degradation (8). Due to the increased lysosomal turnover of CI-M6PR in dysfunctional retromer trafficking, protein levels of CI-M6PR, the best characterized retromer cargo, are reduced at steady state. Moreover, mutations in the retromer component VPS35 have been linked to PD (59,60) and reduced levels of cellular CI-M6PR have been reported in studies of PD genes including VPS35 (13,41), LRRK2 (34), Rab7L1 (61), and Parkin (62), highlighting retromer dysfunction in PD pathogenesis (63). In the present study, we found that the distribution of the retromer complex component VPS35 was disrupted in cells expressing PD-linked TME230 mutants (R141L and *184Wext*5), and that cellular levels of the retromer cargo CI-M6PR were reduced upon TMEM230 knockdown or R141L-TMEM230 expression. We also demonstrated that Rab8a is necessary for maintenance of normal CI-M6PR protein levels. Although further studies will be required to elucidate the molecular mechanism by which the loss of functions of TMEM230 and LRRK2 lead to reduced CI-M6PR protein levels, our data suggest that reduced Rab8a protein levels in TMEM230 knockdown cells, and altered Rab8a phosphorylation (or activation cycling) in LRRK2 knockdown cells may contribute at least in part to retromer dysfunction.

In summary, our study demonstrates a novel role for TMEM230 in regulating both retromer trafficking and the secretory pathway. Thus, it will be of interest to further investigate the mechanistic interplay between these two closely-related pathways in the pathogenesis of PD.

## Materials and Methods

### Antibodies and chemicals

The following antibodies were used in immunoblot analysis or immunostaining: anti-GFP (Cell Signaling, #2956), anti-FLAG (Sigma, #F7425), anti-TMEM230 (Origene, #TA504888), anti-CI-M6PR (Abcam, #ab124767E9644), anti-VPS35 (SantaCruz, #sc-374372), anti-tubulin (Sigma #T5168), anti-p62 (Sigma, #P0067), anti-α-synuclein (Santa Cruz #sc-7011-R), anti-Mfn1 (Cell Signaling, #13196), anti-LC3 (Cell Signaling, #3868), anti-cathepsin-D (Santa Cruz, #sc-6478), anti-HEX-B (Santa Cruz, #sc-376781), anti-Rab8a (Proteintech, #55296-1-AP), anti-Rab7a (Sigma, #R4779), anti-LRRK2 (NeuroMab, #75-253). Bafilomycin-A1 (Baf-A1) and Carbonyl cyanide *m*-chlorophenylhydrazone

(CCCP) were purchased from Cayman chemicals. Other chemicals were purchased from Sigma, unless otherwise stated.

### Plasmids

Tag-free TMEM230 expression vectors are previously described (6). FLAG-VPS35 was a generous gift from Dr. Fumio Kishi (Kawasaki Medical School, Japan) (58). The following lentiviral RNAi were purchased from GE-healthcare Life Sciences: TMEM230-RNAi (TRCN0000129581 (target sequence-5'-CCAGTGCTGATCATTGGCATT-3') and TRCN0000131231 (target sequence- 5'-GACGATGGCTACATTGACCTT-3')), Rab8a-RNAi (TRCN0000048215 (target sequence- 5'-CGAGAAGTCCTT CGACAACAT-3')), LRRK2-RNAi (TRCN0000021461 (target sequence- 5'-GCCAGAGGAAATGTCATTTAT-3')). As a control, pLKO.1 with a nontargeting shRNA insert (5'-CCT AAG GTT AAG TCG CCC TCG CTC GAG CGA GGG CGA CTT AAC CTT AGG-3') was used. pGFP-Rab8A (Addgene Plasmid #24898) and pGFP-Rab8A-[T22N] (Addgene Plasmid #24899) were gifts from Dr. Maxence Nachury (Stanford University School of Medicine, CA).

### Cell culture and transfection

Human embryonic kidney (HEK) cell line 293FT (Life Technologies) and African green monkey kidney fibroblast (COS-7) cells were maintained in Dulbecco's modified Eagle's Medium (DMEM) supplemented with 10% FBS (Life Technologies), 100 U/ml penicillin, and 100 μg/ml streptomycin at 37 °C with 5% $CO_2$ incubation. Cells were plated one day prior to transfection in 12-well plates (Corning) at a density of approximately 125,000 cells per 12-well. Transfections were performed with Lipofectamine 2000 (Invitrogen) according to the manufacturer's recommended protocol. Human lymphoblastoid cell lines were maintained in RPMI-1640 supplemented with 10% FBS, 100 U/ml penicillin, and 100 μg/ml streptomycin at 37 °C with 5% $CO_2$ incubation.

### Lentivirus preparation and generation of HEK293-FT cells expressing either TMEM230-RNAi or Scr-RNAi

For the production of lentiviral vectors, a 15 cm tissue culture dish containing 70% confluent HEK293FT cells was transfected with 10 μg of transfer vector (TMEM230-RNAi in pLKO.1 (TRCN0000131231) or control Scr-RNAi in pLKO.1), 9 μg psPAX2, and 1 μg VSVG using Lipofectamine2000 according to manufacturer's protocol for 16–18 h. The medium was then replaced into DMEM containing 10% fetal bovine serum and 1% Pen/Strep (Invitrogen). The virus was harvested 2 days post-transfection. The collected supernatant containing the virus was briefly spun at 1000 rpm and filtered through a 0.45 μm filter. The resulting virus mixture was concentrated at 80X with LentiX-concentrator reagent (Clontech), according to the manufacturer's protocol. The pellet containing the virus was resuspended with DMEM medium (Invitrogen) and frozen for future use. For the generation of stable HEK293-FT cell line expressing RNAi constructs, HEK293-FT cells in 6-well plates were infected with 1.5 μl of viral resuspension. HEK293-FT cells expressing either TMEM230-RNAi or Scr-RNAi were selected using puromycin (2 μg/mL).

### Preparations of extracellular media fraction and cell lysates fraction

Transfected HEK293-FT cells in 12-wells were left untreated or treated with Baf-A1 (300 nM) for the indicated times at 37 °C with 5% $CO_2$ incubation. Cells were then chilled on ice for 5 min. 0.9 ml of extracellular media samples from each 12-well were transferred to 1.5 ml tubues, and spun for 15 min at 550Xg in 4°C to remove cell debris. Subsequently 0.75 ml from the cleared media were transferred to new 1.5 ml tubes, and then the media samples were spun for 30 min at 2500Xg in 4°C. After the centrifugation, 0.5 ml of extracellular media samples were transferred to fresh 1.5 ml tubes for immunoblot analysis. For immunoblot analysis of extracellular media samples, 100 μl of cleared extracellular media samples from 2500xg spin were mixed with 100 μl of 4X SDS sample buffer (200 mM Tris-Cl (pH 6.8), 8% (w/v) SDS, 0.1% (w/v) bromophenol blue, 40% (v/v) glycerol, 400 mM DTT (dithiothreitol)) and boiled for 10 min. For the preparation of cell lysate fraction, cells on culture plates were washed once with PBS and lysed with 300 ml of 2X SDS-sample buffer.

### Immunoblotting

Protein samples were subjected to SDS-PAGE. Proteins were then transferred to polyvinylidene fluoride (PVDF) or nitrocellulose membranes using Trans-Blot Turbo Transfer system (Bio-Rad). The membranes were incubated overnight with the indicated primary antibodies. All primary antibodies were diluted in an antibody dilution buffer (25 mM Tris, 0.15 M NaCl, 0.05% Tween-20, 5% BSA, 0.05% sodium azide). Primary antibodies were visualized using the appropriate horseradish peroxidase conjugated secondary antibody (anti-mouse (Jackson immunoresearch lab, #115-035-146), anti-rabbit (Jackson immunoresearch lab, #111-035-144) anti-goat (Jackson immunoresearch lab, #805-035-180) and SuperSignal West Femto Maximum Sensitivity Substrate (Thermo Scientific, #34096). Blots were imaged on the ChemiDoc MP System (Bio-Rad) with a 16-bit CCD camera. The signal accumulation mode was used to acquire images at progressively longer exposure times. This allowed for acquisition of western blot images with band intensities within the linear range of the system. Quantification of protein levels was done using Bio-Rad ImageLab software and ImageJ (NIH) using non-saturated raw image files. Data were normalized to tubulin and expressed relative to control levels as indicated.

### Immunostaining and imaging

COS-7 cells grown on cover glass were co-transfected with TMEM230 expression vectors and FLAG-VPS35. One day after transfection, COS-7 cells were fixed with 4% formaldehyde in PBS for 10 min. After fixation, cells were washed three times for 30 min at room temperature, and incubated with primary antibodies (rabbit anti-FLAG and mouse anti-TMEM230 antibody) in GDB buffer (30 mM phosphate buffer, pH 7.4, containing 0.1% gelatin, 0.3% Triton X-100, and 0.45 M NaCl) overnight at 4°C. Cells were then washed three times in PBS for 30 min at room temperature and incubated with secondary antibody conjugated to Alexa-488 and Alexa-568 in GDB for 1 hr at room temperature and washed three times in PBS for 30 min. Images were taken with a Leica epifluorescence microscope with 40x air objective.

### Statistics

All values in figures and text refer to mean ± SEM unless otherwise stated. N refers to the number of independent experiments unless otherwise indicated. Statistics and graphing were performed using Prism (GraphPad) software. Statistical analysis of data was performed with two-tailed paired *t*-test unless otherwise indicated.

## Supplementary Material

Supplementary Material is available at *HMG* online.

## Acknowledgements

We thank Dr Fumio Kishi (Kawasaki Medical School, Japan) for the FLAG-VPS35 construct. We thank Hyunkyung Jeong for helpful comments on this manuscript.

*Conflict of Interest statement*. None declared.

## Funding

NIH grant (R01NS076054 to D.K., R01NS099623 to H.D., R21 NS074366 to H.D., NS050641 to T.S.); Les Turner ALS Foundation Professorship (T.S.).

## References

1. Kalia, L.V. and Lang, A.E. (2015) Parkinson's disease. *Lancet*, **386**, 896–912.
2. Bras, J., Guerreiro, R. and Hardy, J. (2015) SnapShot: Genetics of Parkinson's disease. *Cell*, **160**, 570-570. e571.
3. Gasser, T. (2009) Molecular pathogenesis of Parkinson disease: insights from genetic studies. *Expert Rev. Mol. Med.*, **11**, e22.
4. Simon-Sanchez, J., Schulte, C., Bras, J.M., Sharma, M., Gibbs, J.R., Berg, D., Paisan-Ruiz, C., Lichtner, P., Scholz, S.W., Hernandez, D.G., *et al.* (2009) Genome-wide association study reveals genetic risk underlying Parkinson's disease. *Nat. Genet.*, **41**, 1308–1312.
5. Michel, P.P., Hirsch, E.C. and Hunot, S. (2016) Understanding Dopaminergic Cell Death Pathways in Parkinson Disease. *Neuron*, **90**, 675–691.
6. Deng, H.X., Shi, Y., Yang, Y., Ahmeti, K.B., Miller, N., Huang, C., Cheng, L., Zhai, H., Deng, S., Nuytemans, K., *et al.* (2016) Identification of TMEM230 mutations in familial Parkinson's disease. *Nat. Genet.*, **48**, 733–739.
7. Steger, M., Tonelli, F., Ito, G., Davies, P., Trost, M., Vetter, M., Wachter, S., Lorentzen, E., Duddy, G., Wilson, S., *et al.* (2016) Phosphoproteomics reveals that Parkinson's disease kinase LRRK2 regulates a subset of Rab GTPases. *Elife*, **5**,
8. Arighi, C.N., Hartnell, L.M., Aguilar, R.C., Haft, C.R. and Bonifacino, J.S. (2004) Role of the mammalian retromer in sorting of the cation-independent mannose 6-phosphate receptor. *J. Cell Biol.*, **165**, 123–133.
9. Cullen, P.J. and Korswagen, H.C. (2012) Sorting nexins provide diversity for retromer-dependent trafficking events. *Nat. Cell Biol.*, **14**, 29–37.
10. Gallon, M. and Cullen, P.J. (2015) Retromer and sorting nexins in endosomal sorting. *Biochem. Soc. Trans.*, **43**, 33–47.
11. Braulke, T. and Bonifacino, J.S. (2009) Sorting of lysosomal proteins. *Biochim. Biophys. Acta*, **1793**, 605–614.
12. Follett, J., Norwood, S.J., Hamilton, N.A., Mohan, M., Kovtun, O., Tay, S., Zhe, Y., Wood, S.A., Mellick, G.D., Silburn, P.A., *et al.* (2014) The Vps35 D620N mutation linked to Parkinson's disease disrupts the cargo sorting function of retromer. *Traffic*, **15**, 230–244.
13. Miura, E., Hasegawa, T., Konno, M., Suzuki, M., Sugeno, N., Fujikake, N., Geisler, S., Tabuchi, M., Oshima, R., Kikuchi, A., *et al.* (2014) VPS35 dysfunction impairs lysosomal degradation of alpha-synuclein and exacerbates neurotoxicity in a Drosophila model of Parkinson's disease. *Neurobiol. Dis.*, **71**, 1–13.
14. Yoshimori, T., Yamamoto, A., Moriyama, Y., Futai, M. and Tashiro, Y. (1991) Bafilomycin A1, a specific inhibitor of vacuolar-type H(+)-ATPase, inhibits acidification and protein degradation in lysosomes of cultured cells. *J. Biol. Chem.*, **266**, 17707–17712.
15. Beilina, A. and Cookson, M.R. (2015) Genes associated with Parkinson's disease: regulation of autophagy and beyond. *J. Neurochem*, 139 Suppl 1:91–107.
16. Xilouri, M., Brekk, O.R. and Stefanis, L. (2016) Autophagy and Alpha-Synuclein: Relevance to Parkinson's Disease and Related Synucleopathies. *Mov. Disord.*, **31**, 178–192.
17. Gegg, M.E., Cooper, J.M., Chau, K.Y., Rojo, M., Schapira, A.H. and Taanman, J.W. (2010) Mitofusin 1 and mitofusin 2 are ubiquitinated in a PINK1/parkin-dependent manner upon induction of mitophagy. *Hum. Mol. Genet.*, **19**, 4861–4870.
18. Youle, R.J. and Narendra, D.P. (2011) Mechanisms of mitophagy. *Nat. Rev. Mol. Cell Biol.*, **12**, 9–14.
19. Klionsky, D.J., Abdelmohsen, K., Abe, A., Abedin, M.J., Abeliovich, H., Acevedo Arozena, A., Adachi, H., Adams, C.M., Adams, P.D., Adeli, K., *et al.* (2016) Guidelines for the use and interpretation of assays for monitoring autophagy (3rd edition). *Autophagy*, **12**, 1–222.
20. Tapper, H. and Sundler, R. (1995) Bafilomycin A1 inhibits lysosomal, phagosomal, and plasma membrane H(+)-ATPase and induces lysosomal enzyme secretion in macrophages. *J. Cell Physiol.*, **163**, 137–144.
21. Camacho, M., Machado, J.D., Alvarez, J. and Borges, R. (2008) Intravesicular calcium release mediates the motion and exocytosis of secretory organelles: a study with adrenal chromaffin cells. *J. Biol. Chem.*, **283**, 22383–22389.
22. Taupenot, L., Harper, K.L. and O'Connor, D.T. (2005) Role of H+-ATPase-mediated acidification in sorting and release of the regulated secretory protein chromogranin A: evidence for a vesiculogenic function. *J. Biol. Chem.*, **280**, 3885–3897.
23. Dupont, N., Jiang, S., Pilli, M., Ornatowski, W., Bhattacharya, D. and Deretic, V. (2011) Autophagy-based unconventional secretory pathway for extracellular delivery of IL-1beta. *Embo J.*, **30**, 4701–4711.
24. Duran, J.M., Anjard, C., Stefan, C., Loomis, W.F. and Malhotra, V. (2010) Unconventional secretion of Acb1 is mediated by autophagosomes. *J. Cell Biol.*, **188**, 527–536.
25. Ejlerskov, P., Rasmussen, I., Nielsen, T.T., Bergstrom, A.L., Tohyama, Y., Jensen, P.H. and Vilhardt, F. (2013) Tubulin polymerization-promoting protein (TPPP/p25alpha) promotes unconventional secretion of alpha-synuclein through exophagy by impairing autophagosome-lysosome fusion. *J. Biol. Chem.*, **288**, 17313–17335.
26. Jiang, S., Dupont, N., Castillo, E.F. and Deretic, V. (2013) Secretory versus degradative autophagy: unconventional secretion of inflammatory mediators. *J. Innate Immun.*, **5**, 471–479.
27. Ponpuak, M., Mandell, M.A., Kimura, T., Chauhan, S., Cleyrat, C. and Deretic, V. (2015) Secretory autophagy. *Curr. Opin. Cell Biol.*, **35**, 106–116.

28. Son, S.M., Cha, M.Y., Choi, H., Kang, S., Choi, H., Lee, M.S., Park, S.A. and Mook-Jung, I. (2016) Insulin-degrading enzyme secretion from astrocytes is mediated by an autophagy-based unconventional secretory pathway in Alzheimer disease. *Autophagy*, **12**, 784–800.
29. Pfeffer, S.R. (2013) Rab GTPase regulation of membrane identity. *Curr. Opin. Cell Biol.*, **25**, 414–419.
30. Stenmark, H. (2009) Rab GTPases as coordinators of vesicle traffic. *Nat. Rev. Mol. Cell Biol.*, **10**, 513–525.
31. Huber, L.A., Pimplikar, S., Parton, R.G., Virta, H., Zerial, M. and Simons, K. (1993) Rab8, a small GTPase involved in vesicular traffic between the TGN and the basolateral plasma membrane. *J. Cell Biol.*, **123**, 35–45.
32. Paisan-Ruiz, C., Jain, S., Evans, E.W., Gilks, W.P., Simon, J., van der Brug, M., Lopez de Munain, A., Aparicio, S., Gil, A.M., Khan, N., *et al.* (2004) Cloning of the gene containing mutations that cause PARK8-linked Parkinson's disease. *Neuron*, **44**, 595–600.
33. Zimprich, A., Biskup, S., Leitner, P., Lichtner, P., Farrer, M., Lincoln, S., Kachergus, J., Hulihan, M., Uitti, R.J., Calne, D.B., *et al.* (2004) Mutations in LRRK2 cause autosomal-dominant parkinsonism with pleomorphic pathology. *Neuron*, **44**, 601–607.
34. MacLeod, D.A., Rhinn, H., Kuwahara, T., Zolin, A., Di Paolo, G., McCabe, B.D., Marder, K.S., Honig, L.S., Clark, L.N., Small, S.A., *et al.* (2013) RAB7L1 interacts with LRRK2 to modify intraneuronal protein sorting and Parkinson's disease risk. *Neuron*, **77**, 425–439.
35. Dehay, B., Martinez-Vicente, M., Caldwell, G.A., Caldwell, K.A., Yue, Z., Cookson, M.R., Klein, C., Vila, M. and Bezard, E. (2013) Lysosomal impairment in Parkinson's disease. *Mov. Disord.*, **28**, 725–732.
36. Frake, R.A., Ricketts, T., Menzies, F.M. and Rubinsztein, D.C. (2015) Autophagy and neurodegeneration. *J. Clin. Invest.*, **125**, 65–74.
37. Gan-Or, Z., Dion, P.A. and Rouleau, G.A. (2015) Genetic perspective on the role of the autophagy-lysosome pathway in Parkinson disease. *Autophagy*, **11**, 1443–1457.
38. Menzies, F.M., Fleming, A. and Rubinsztein, D.C. (2015) Compromised autophagy and neurodegenerative diseases. *Nat. Rev. Neurosci.*, **16**, 345–357.
39. Alegre-Abarrategui, J., Christian, H., Lufino, M.M., Mutihac, R., Venda, L.L., Ansorge, O. and Wade-Martins, R. (2009) LRRK2 regulates autophagic activity and localizes to specific membrane microdomains in a novel human genomic reporter cellular model. *Hum. Mol. Genet.*, **18**, 4022–4034.
40. Cuervo, A.M., Stefanis, L., Fredenburg, R., Lansbury, P.T. and Sulzer, D. (2004) Impaired degradation of mutant alpha-synuclein by chaperone-mediated autophagy. *Science*, **305**, 1292–1295.
41. Tang, F.L., Erion, J.R., Tian, Y., Liu, W., Yin, D.M., Ye, J., Tang, B., Mei, L. and Xiong, W.C. (2015) VPS35 in Dopamine Neurons Is Required for Endosome-to-Golgi Retrieval of Lamp2a, a Receptor of Chaperone-Mediated Autophagy That Is Critical for alpha-Synuclein Degradation and Prevention of Pathogenesis of Parkinson's Disease. *J. Neurosci.*, **35**, 10613–10628.
42. Tong, Y., Giaime, E., Yamaguchi, H., Ichimura, T., Liu, Y., Si, H., Cai, H., Bonventre, J.V. and Shen, J. (2012) Loss of leucine-rich repeat kinase 2 causes age-dependent bi-phasic alterations of the autophagy pathway. *Mol. Neurodegener.*, **7**, 2.
43. Tong, Y., Yamaguchi, H., Giaime, E., Boyle, S., Kopan, R., Kelleher, R.J., 3rd. and Shen, J. (2010) Loss of leucine-rich repeat kinase 2 causes impairment of protein degradation pathways, accumulation of alpha-synuclein, and apoptotic cell death in aged mice. *Proc. Natl Acad. Sci. U S A*, **107**, 9879–9884.
44. Vogiatzi, T., Xilouri, M., Vekrellis, K. and Stefanis, L. (2008) Wild type alpha-synuclein is degraded by chaperone-mediated autophagy and macroautophagy in neuronal cells. *J. Biol. Chem.*, **283**, 23542–23556.
45. Yin, G., Lopes da Fonseca, T., Eisbach, S.E., Anduaga, A.M., Breda, C., Orcellet, M.L., Szego, E.M., Guerreiro, P., Lazaro, D.F., Braus, G.H., *et al.* (2014) alpha-Synuclein interacts with the switch region of Rab8a in a Ser129 phosphorylation-dependent manner. *Neurobiol. Dis.*, **70**, 149–161.
46. Lai, Y.C., Kondapalli, C., Lehneck, R., Procter, J.B., Dill, B.D., Woodroof, H.I., Gourlay, R., Peggie, M., Macartney, T.J., Corti, O., *et al.* (2015) Phosphoproteomic screening identifies Rab GTPases as novel downstream targets of PINK1. *Embo J.*, **34**, 2840–2861.
47. Gitler, A.D., Bevis, B.J., Shorter, J., Strathearn, K.E., Hamamichi, S., Su, L.J., Caldwell, K.A., Caldwell, G.A., Rochet, J.C., McCaffery, J.M., *et al.* (2008) The Parkinson's disease protein alpha-synuclein disrupts cellular Rab homeostasis. *Proc. Natl Acad. Sci. U S A*, **105**, 145–150.
48. Alvarez-Erviti, L., Seow, Y., Schapira, A.H., Gardiner, C., Sargent, I.L., Wood, M.J. and Cooper, J.M. (2011) Lysosomal dysfunction increases exosome-mediated alpha-synuclein release and transmission. *Neurobiol. Dis.*, **42**, 360–367.
49. Danzer, K.M., Kranich, L.R., Ruf, W.P., Cagsal-Getkin, O., Winslow, A.R., Zhu, L., Vanderburg, C.R. and McLean, P.J. (2012) Exosomal cell-to-cell transmission of alpha synuclein oligomers. *Mol. Neurodegener.*, **7**, 42.
50. Tsunemi, T., Hamada, K. and Krainc, D. (2014) ATP13A2/PARK9 regulates secretion of exosomes and alpha-synuclein. *J. Neurosci.*, **34**, 15281–15287.
51. Paillusson, S., Clairembault, T., Biraud, M., Neunlist, M. and Derkinderen, P. (2013) Activity-dependent secretion of alpha-synuclein by enteric neurons. *J. Neurochem.*, **125**, 512–517.
52. Lee, H.J., Patel, S. and Lee, S.J. (2005) Intravesicular localization and exocytosis of alpha-synuclein and its aggregates. *J. Neurosci.*, **25**, 6016–6024.
53. Langston, J.W., Schule, B., Rees, L., Nichols, R.J. and Barlow, C. (2015) Multisystem Lewy body disease and the other parkinsonian disorders. *Nat. Genet.*, **47**, 1378–1384.
54. Ross, O.A., Toft, M., Whittle, A.J., Johnson, J.L., Papapetropoulos, S., Mash, D.C., Litvan, I., Gordon, M.F., Wszolek, Z.K., Farrer, M.J., *et al.* (2006) Lrrk2 and Lewy body disease. *Ann. Neurol.*, **59**, 388–393.
55. Spillantini, M.G., Schmidt, M.L., Lee, V.M., Trojanowski, J.Q., Jakes, R. and Goedert, M. (1997) Alpha-synuclein in Lewy bodies. *Nature*, **388**, 839–840.
56. Baptista, M.A., Dave, K.D., Frasier, M.A., Sherer, T.B., Greeley, M., Beck, M.J., Varsho, J.S., Parker, G.A., Moore, C., Churchill, M.J., *et al.* (2013) Loss of leucine-rich repeat kinase 2 (LRRK2) in rats leads to progressive abnormal phenotypes in peripheral organs. *PLoS One*, **8**, e80705.
57. Beilina, A., Rudenko, I.N., Kaganovich, A., Civiero, L., Chau, H., Kalia, S.K., Kalia, L.V., Lobbestael, E., Chia, R., Ndukwe, K., *et al.* (2014) Unbiased screen for interactors of leucine-rich repeat kinase 2 supports a common pathway for sporadic and familial Parkinson disease. *Proc. Natl Acad. Sci. U S A*, **111**, 2626–2631.
58. Tabuchi, M., Yanatori, I., Kawai, Y. and Kishi, F. (2010) Retromer-mediated direct sorting is required for proper endosomal recycling of the mammalian iron transporter DMT1. *J. Cell Sci.*, **123**, 756–766.

59. Vilarino-Guell, C., Wider, C., Ross, O.A., Dachsel, J.C., Kachergus, J.M., Lincoln, S.J., Soto-Ortolaza, A.I., Cobb, S.A., Wilhoite, G.J., Bacon, J.A., *et al.* (2011) VPS35 mutations in Parkinson disease. *Am. J. Hum. Genet.*, **89**, 162–167.
60. Zimprich, A., Benet-Pages, A., Struhal, W., Graf, E., Eck, S.H., Offman, M.N., Haubenberger, D., Spielberger, S., Schulte, E.C., Lichtner, P., *et al.* (2011) A mutation in VPS35, encoding a subunit of the retromer complex, causes late-onset Parkinson disease. *Am. J. Hum. Genet.*, **89**, 168–175.
61. Wang, S., Ma, Z., Xu, X., Wang, Z., Sun, L., Zhou, Y., Lin, X., Hong, W. and Wang, T. (2014) A role of Rab29 in the integrity of the trans-Golgi network and retrograde trafficking of mannose-6-phosphate receptor. *PLoS One*, **9**, e96242.
62. Song, P., Trajkovic, K., Tsunemi, T. and Krainc, D. (2016) Parkin Modulates Endosomal Organization and Function of the Endo-Lysosomal Pathway. *J. Neurosci.*, **36**, 2425–2437.
63. Small, S.A. and Petsko, G.A. (2015) Retromer in Alzheimer disease, Parkinson disease and other neurological disorders. *Nat. Rev. Neurosci.*, **16**, 126–132.